NANO LETTERS

pubs.acs.org/NanoLett Letter

Strain-Tunable Hyperbolic Exciton Polaritons in Monolayer Black Arsenic with Two Exciton Resonances

Hongwei Wang,* Yuhan Zhong, Wei Jiang, Simone Latini, Shengxuan Xia, Tian Cui,* Zhenglu Li, Tony Low,* and Feng Liu*

Cite This: *Nano Lett.* 2024, 24, 2057−2062 Read Online

ACCESS | Metrics & More | Article Recommendations | Supporting Information

ABSTRACT: Hyperbolic polaritons have been attracting increasing interest for applications in optoelectronics, biosensing, and super-resolution imaging. Here, we report the in-plane hyperbolic exciton polaritons in monolayer black-arsenic (B-As), where hyperbolicity arises strikingly from two exciton resonant peaks. Remarkably, the presence of two resonances at different momenta makes overall hyperbolicity highly tunable by strain, as the two exciton peaks can be merged into the same frequency to double the strength of hyperbolicity as well as light absorption under a 1.5% biaxial strain. Moreover, the frequency of the merged hyperbolicity can be further tuned from 1.35 to 0.8 eV by an anisotropic biaxial strain. Furthermore, electromagnetic numerical simulation reveals a strain-induced hyperbolicity, as manifested in a topological transition of iso-frequency contour of exciton polaritons. The good tunability, large exciton binding energy, and strong light absorption exhibited in the hyperbolic monolayer B-As make it highly suitable for nanophotonics applications under ambient conditions.

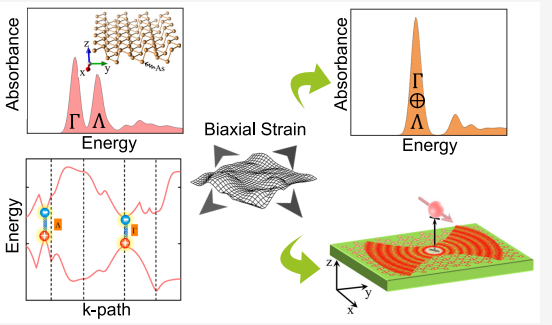

KEYWORDS: *Excitons, Hyperbolic materials, Two-dimensional materials, First-principles method*

Two-dimensional (2D) van der Waals (vdW) materials have attracted great attention due to their rich physical properties originated from their reduced dimensionality[1] and potential in optoelectronic[2,3] and spintronic applications.[4] The quantum confinement and reduced Coulomb screening in 2D lead to enhanced Coulomb interactions giving rise to formation of strongly bounded excitons,[5,6] whose binding energies are generally 1−2 orders of magnitude larger than in 3D semiconductors like GaAs[7] and can even exceed the band gap predicted to realize the elusive excitonic insulator state[8] and excitonic Bose Einstein condensation.[9] Experiment shows light absorption from the lowest excitonic resonance is extremely strong in 2D vdW transition metal dichalcogenides (TMDs),[10] up to 15% of incoming light at the atomically thin limit. Furthermore, the properties of 2D excitons can be effectively tailored by strain engineering[11,12] via interlayer twist and/or lattice mismatch in forming heterostructures.[7,13−15]

In recent years, diverse polaritons, originating from the coupling of electromagnetic fields with electric dipoles, have been discovered in vdW materials,[16,17] in association with plasmons,[18,19] phonons,[20] and excitons,[21,22] as well as their hybrids.[23−25] Especially, exciton polaritons in 2D systems can exhibit intriguing optical phenomena, such as the hyperbolic dispersion that stems from highly anisotropic optical permittivity which changes sign along different crystallographic axes.[26] The hyperbolic polaritons allow for extremely strong electromagnetic confinements and high density of states, providing promising applications for subdiffractional focusing,[27] wave-guiding,[28] biosensing,[29] and quantum photonics.[30]

Naturally, a hyperbolic exciton polariton emerges from some form of structural anisotropy. It was first experimentally observed in the layered TMD WSe_2,[31] arising from the anisotropy between the basal plane and out-of-plane **z**-axis. Also, monolayer black phosphorus (B-P) with strong in-plane anisotropy[32] is found to host a hyperbolic exciton polariton, whose intensity and frequency vary with the increasing film thickness. On the other hand, hyperbolicity is defined with one single exciton resonance, which occurs usually at a high-symmetry **k**-point in most materials, such as the Γ-point for B-P. This apparently limits both the availability and tunability of hyperbolic exciton polaritons. In general, the emerging field of hyperbolic exciton polaritons is still in its infancy; it is highly desirable to discover 2D materials that host strong and tunable hyperbolic exciton polaritons to facilitate their potential applications.

In this study, we report the discovery of in-plane hyperbolic exciton polaritons in monolayer black-arsenic (B-As) which

Received: December 4, 2023
Revised: January 22, 2024
Accepted: January 22, 2024
Published: January 29, 2024

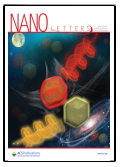

https://doi.org/10.1021/acs.nanolett.3c04730
Nano Lett. 2024, 24, 2057−2062

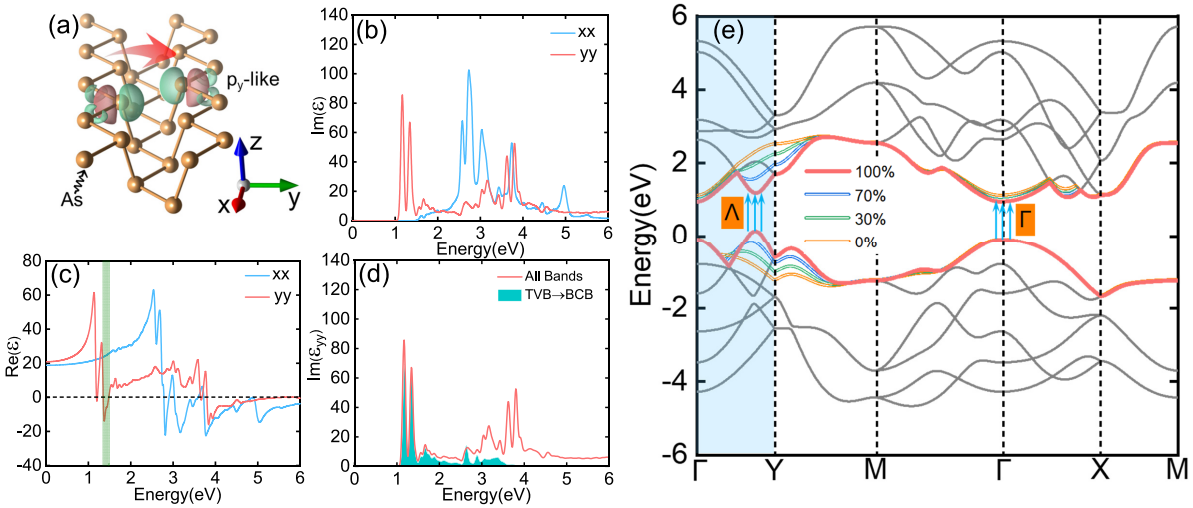

Figure 1. Optical dielectric function and electronic structure of monolayer B-As. (a) Schematic illustration of the crystal structure and its interchain hopping between p_y-like Wannier orbitals. (b) Imaginary part and (c) real part of the dielectric function plotted with a broadening parameter of 40 meV. (d) Comparison of the imaginary part of the dielectric function for the full-band transitions and the transition between top valence and bottom conduction bands. (e) The variation of band dispersion in the vicinity of the Λ point with the interchain hopping integral changed artificially from 100% to 0%. The band structures are calculated based on the conventional density-functional theory within the generalized gradient approximations (GGAs).

was reported to exbibit extreme in-plane anisotropy in electronic, thermal, and electric transport properties, as well as a relatively good ambient stability.[33,34] As a pleasant surprise, the hyperbolicity in B-As was found to arise strikingly from two exciton resonant peaks, in contrast to one peak found previously. Particularly, one additional peak occurs at a low-symmetry **k**-point, instead of the commonly seen peak at a high-symmetry **k**-point. The additional exciton resonance is revealed to arise from strong interchain hoppings between p_y orbitals, a distinctive feature possessed by monolayer B-As with weak sp hybridization. Most importantly, the presence of two resonances enables the hyperbolicity to be highly tunable by strain in both strength and frequency. The two exciton peaks can be merged into the same frequency to double the overall strength of hyperbolicity and light absorption under biaxial tensile strain, much higher than those previously found in monolayer TMDs and B-P. Moreover, the frequency of the merged hyperbolic resonance can be tuned over a large range from visible to near-infrared by applying an additional anisotropic biaxial strain.

Monolayer B-As has an orthorhombic pleated honeycomb structure in which each As atom is coordinated to three neighboring atoms.[33] Here, two in-plane principal axes, zigzag and armchair, are designated respectively as **x** and **y** directions, as illustrated in Figure 1a. To reveal excitonic effects in B-As, we perform optical simulations by ab initio many-body perturbation theory calculations within the GW approximation[35] and the Bethe−Salpeter equation (BSE).[36,37] Parts b and c of Figure 1 show the calculated imaginary and real parts of dielectric functions, respectively. Notably, one sees two sharp exciton resonant peaks at 1.17 and 1.35 eV in Figure 1b. The oscillator strengths of the two excitonic peaks are very strong in the **y** direction but minimal in the **x** direction, indicative of strong optical anisotropy. According to the Kramers−Kronig relation, the strong absorption peak at a given resonant frequency would result in a negative permittivity close to this frequency.[19] Figure 1c shows that the high-energy excitonic peak in Figure 1b gives a sizable negative permittivity in the **y** direction; meanwhile, the low-energy excitonic peak leads to a weak negative permittivity in the **y** direction. The negative permittivity at low energy is counterbalanced by a significant positive permittivity induced by the high-energy resonant peak due to the interference between the two closely spaced exciton resonances. In contrast, the permittivity in the **x** direction is positive and varies smoothly below 1.5 eV (Figure 1c). Consequently, the sign-changing optical permittivity along the two in-plane principal axes is expected to generate one prominent hyperbolic region, highlighted by the green shadow in Figure 1c, and one relatively weaker hyperbolic region.

To identify the origin of exciton resonances in monolayer B-As, we perform band decomposition analysis for the optical transitions. Figure 1d shows the imaginary parts of dielectric functions in the **y** direction contributed by full transition involving all valence and conduction bands versus partial transition involving only between the top valence band (TVB) and the bottom conduction band (BCB). The transition between TVB and BCB is found to be sufficient to capture the overall excitonic signature in the low-energy region. The two exciton resonant peaks originate from band edges of the TVB and BCB at the Γ point and Λ point in the Γ−Y **k**-path, respectively, as shown in Figure 1e (see also Figure S1 in the Supporting Information). Here, we just focus on the band dispersion near the Fermi level; thus, the band structures in Figure 1e are calculated with exchange correlation energy using the generalized gradient approximations (GGAs) instead of GW approximations to circumvent expensive computational cost. The electron and hole are inclined to bind, forming an exciton at the conduction band minimum and the valence band maximum at the same **k** point, in conjunction with the parabolic dispersion around the extrema. For comparison, monolayer B-P possesses only one parabolic band extrema at the Γ point (Figure S1), and hence only one exciton resonant peak in the optical absorption spectra.[32]

Interestingly, although B-As and B-P adopt a similar crystal structure, B-As develops an additional parabolic band extrema

https://doi.org/10.1021/acs.nanolett.3c04730
Nano Lett. 2024, 24, 2057−2062

at the Λ point. To understand this intriguing difference, we employ a tight-binding model to analyze the relationship between band dispersion and the orbital interaction. The model Hamiltonian is constructed in the subspace expanded by 12 p orbitals, constructed as the maximally localized Wannier functions.[38] We found that the band dispersion of TVB and BCB at the low-symmetry Λ point in B-As is very sensitive to the interchain hopping of p_y orbitals, as illustrated in Figure 1a. The variation of the band dispersion of TVB and BCB with the interchain hopping integral is shown in Figure 1e. Evidently, the parabolic band extrema at Λ gradually disappear when the interchain hopping is *artificially* reduced. Thus, the additional exciton resonant peak at Λ is attributed to the strong interchain hopping between p_y orbitals in monolayer B-As, which is absent in B-P. This difference is rooted in their different bonding and orbital configurations, as we further elaborate below.

In monolayer B-As, each As atom forms an sp^3-like hybridization to bond with three neighboring atoms with a lone pair of electrons localized at one tetrahedral apex. The lone pair electron exerts a large Coulomb repulsion on the neighboring chemical bonds, resulting in a small bond angle of the tetrahedral unit in B-As (see Figure S2a and d). Indeed, by plotting the electron localization function (Figure S2b and e), we observed that a lone pair of electrons with s-orbital character in B-As is more pronounced than that in B-P. This indicates a weaker s−p hybridization in B-As, so that the p_y orbital can maintain its intrinsic characteristics lying in the basal plane along the **y**-direction (Figure S1c). In contrast, the stronger s−p hybridization in B-P causes the p_y orbital to be oriented away from the basal plane and pointed toward one of the tetrahedral apexes (Figure S1d). The weak s−p hybridization in B-As can be ascribed to the inner orbital contraction caused by the relativistic effect of heavier elements, leading to a larger separation of s and p sub-band energy levels (Figure S2c and f). Consequently, the less hybridized p_y orbital in B-As promotes a larger spatial overlap to enhance interchain electron hopping, which is crucial for generating an extra exciton resonant peak at the Λ point.

Besides the strong exciton resonances, the anisotropic nature of the optical transition in monolayer B-As is a prerequisite for the development of hyperbolicity. The forbidden transition in the **x** direction below 1.5 eV is governed by the selection rule. Monolayer B-As possesses a mirror plane parallel to the **y** direction. Both the initial and final states at the band extrema of the Γ and Λ points exhibit even parity with respect to the mirror plane (Figure S3). As a result, the optical transition is forbidden in the **x** direction. However, there is no such restriction in the **y** direction. This selectivity in optical transition results in a strong anisotropic dielectric environment in B-As.

For technological applications, an important figure-of-merit for the performance of hyperbolic polarization is tunability. In general, excitonic behavior is strongly dependent on the electronic optical gap and band dispersion. Strain engineering has been well established to tune the band structures of semiconductors,[39,40] especially 2D materials[41] which can sustain much larger strain than their 3D counterparts.[42] Here, we explore the effects of strain on the hyperbolicity of excitons. First, we calculated the imaginary and real parts of the dielectric function for monolayer B-As under biaxial strain. We found that the two exciton resonant peaks will undergo an energy separation under a compressive biaxial strain, such as the case of 2.5% strain shown in Figure 2a. This in turn leads to two distinct hyperbolic energy regimes around 0.9 and 1.45

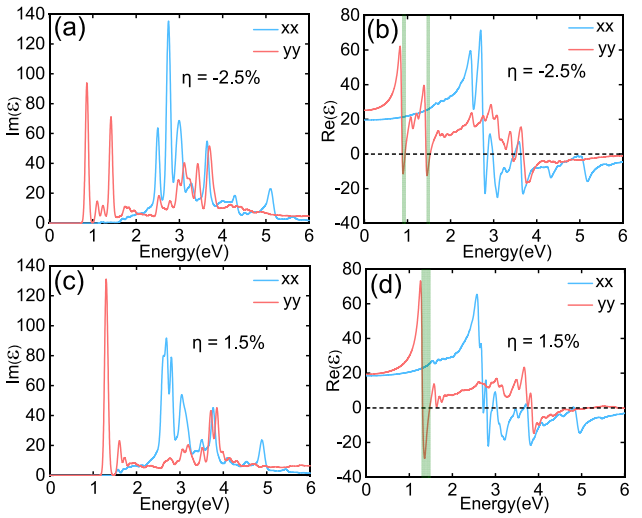

Figure 2. Optical dielectric functions of strained monolayer B-As. (a) Imaginary part and (b) real part of dielectric functions under 2.5% compressive biaxial strain. (c) Imaginary part and (d) real part of dielectric functions under 1.5% tensile biaxial strain. The hyperbolic regimes are highlighted with a green shadow.

eV, respectively, as shown in Figure 2b, and a weakened interference between the two separated exciton resonant peaks. Conversely, applying a tensile biaxial strain drives the two peaks closer. Most interestingly, when 1.5% tensile strain is applied, the two exciton resonant peaks merge to the same frequency being combined into one single strong resonant peak, as shown in Figure 2c. Such enhanced excitonic resonance results in a significant negative permittivity in the hyperbolic energy regime at around 1.35 eV (Figure 2d).

We also applied an anisotropic biaxial strain, in addition to the aforementioned biaxial strain, to further engineer the hyperbolicity of exciton [see details in the Supporting Information (Figure S7)]. Most significantly, the strong combined exciton resonant peak can be tuned from 1.35 to ∼0.8 eV, namely, from the visible to infrared range. This makes it more suitable for practical telecom applications.

As shown in Figure 2a, the oscillator strength of each exciton resonant peak under compressive strain varies only slightly in comparison with the unstrained structure (Figure 1b), and the intensity of the single combined exciton resonant peak under 1.5% tensile strain (Figure 2c) is approximately equal to the sum intensity of the two separate peaks in the pristine state. Therefore, the tunability of excitonic resonances via strain is achieved by almost rigid shifts of two peak positions instead of the oscillator strength. The positions of the exciton resonant peaks in **k**-space are further confirmed by the exciton wave function plots (Figure S6). The exciton resonant peak with lower energy originates from the Γ point, whereas the other peak originates from the Λ point. As shown in Figure 3a, the binding energies of the two excitonic states undergo only minor variations with strain. However, the single-particle bandgap at Γ shows a noticeable increase as a function of strain but remains almost unchanged at Λ. Similar to the trends of the changing bandgap, the position of the exciton peak at Γ exhibits a significant increase with strain, whereas the peak at Λ shows little variation. This indicates that the strain modulated

https://doi.org/10.1021/acs.nanolett.3c04730
Nano Lett. 2024, 24, 2057−2062

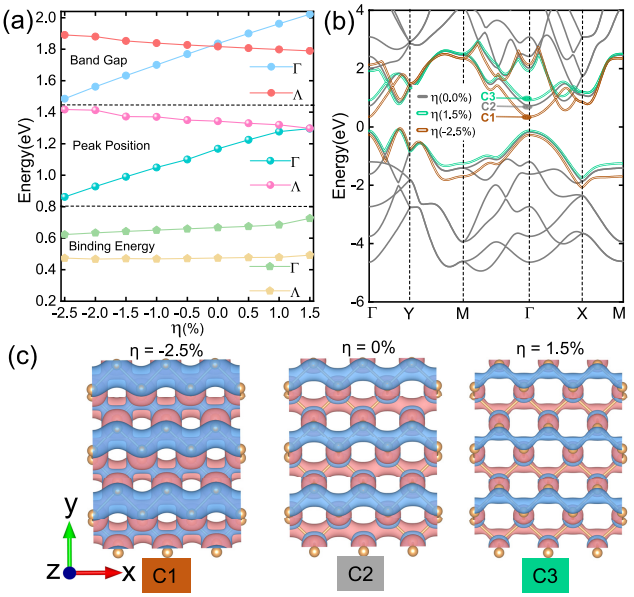

Figure 3. The dependence of band features and exciton properties of monolayer B-As on the applied biaxial strain. (a) Band gap, exciton peak position, and binding energy as a function of the in-plane biaxial strain. (b) Strain modulated band dispersions within GGA in the vicinity of the Fermi level. (c) Top view of wave functions for the bottom conduction band at Γ with and without strain.

bandgap at Γ, causing the shift of the Γ-point exciton resonant peak, plays a crucial role in strain tuning the hyperbolicity of monolayer B-As.

To gain further insight into the relationship between the bandgap and the position of the exciton peak, we analyze band structures under various strain conditions. As shown in Figure 3b, the position of BCB around Γ clearly shifts with strain, accounting for the modulated local Γ-point band gap, while that of TVB remains largely unchanged. In contrast, the band feature around Λ is less affected by strain, consistent with the minor variation observed in the local Λ-point band gap. On the other hand, however, the exciton binding energy is much less sensitive to strain at Γ. It is defined as the energy difference between the peak position and the conduction band minimum (Figure S4), indicating that the position of the exciton peak at Γ is primarily fixed relative to the edge of the BCB. The exciton binding energies at Γ and Λ are further examined using the Mott−Wannier model[43] (see details in the Supporting Information). The difference in binding energy between the two exciton resonant states arises from the distinct exciton reduced masses at the Γ and Λ points (Figure S9), which plays also an important role in inducing two excitonic resonances. Moreover, the exciton binding energy is less sensitive to strain due to the fact that both the effective masses and dielectric screening are less sensitive to strain (see Figures S9 and S10).

The strain induced modulation of the BCB at the Γ point can be understood from a bonding orbital viewpoint. The wave function at the minimum of BCB exhibits bonding character, as shown in Figure 3c, while the next band above BCB displays an antibonding character (Figure S5). It is known that the energy difference between the bonding and antibonding states depends on the degree of orbital hybridization; the larger the hybridization, the larger the difference. Thus, the minimum of BCB with bonding character will be lowered under compressive strain, enhancing orbital hybridization, and raised under tensile strain, weakening orbital hybridization, respectively. Conversely, the next band above BCB with antibonding character displays opposite trends with strain (Figure S5).

Finally, we demonstrate direct strain engineering of hyperbolic exciton polaritons in monolayer B-As, based on dielectric functions calculated from ab initio many-body perturbation theory and electromagnetic numerical simulations. As shown in Figure 4a, the numerically simulated exciton

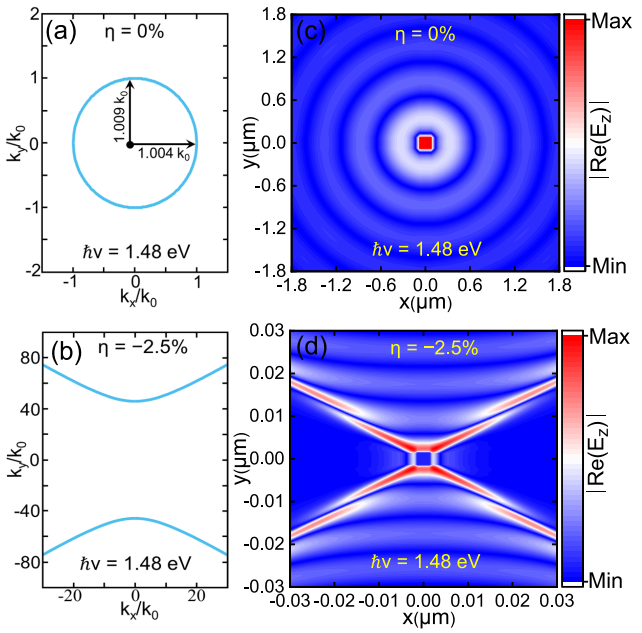

Figure 4. Strain-induced topological transition of the iso-frequency contour of exciton polaritons in monolayer B-As. (a, b) Iso-frequency contours of exciton polaritons at 1.48 eV without strain (a) η = 0% and with strain (b) η = −2.5%. (c, d) The numerically simulated amplitudes of the real part of the near-field distributions at 1.48 eV without strain (c) η = 0% and with strain (d) η = −2.5%.

polariton for pristine monolayer B-As displays an elliptical (closed) dispersion at 1.48 eV, as the permittivities along two in-plane principal axes are both positive. In contrast, under 2.5% compressive strain, the exciton polariton exhibits a hyperbolic (open) dispersion in Figure 4b, due to the strain-tuned negative permittivity in the **y** direction. This signifies a strain-induced hyperbolicity, namely, a topological transition of iso-frequency contour of exciton polaritons at the same frequency. The near-field amplitude distribution in pristine monolayer B-As exhibits an elliptically shaped radial propagation at 1.48 eV (Figure 4c) that matches with the isofrequency dispersion curve in reciprocal space. Then, one can expect that the monolayer B-As under compressive strain can support a concave wavefront for the near-field amplitude distribution (Figure 4d), with the opening direction along the **y** principal axis. Moreover, the numerical simulations reveal that the in-plane hyperbolic polariton can result in high-field confinements with the wavelength up to 52 times smaller than that of free space, which enables focusing and manipulation of electromagnetic waves at a deep subwavelength scale. In addition, the near-field amplitude distribution in monolayer B-As under 1.5% tensile strain also exhibits hyperbolic propagation behavior with evident light confinement at 1.4 eV. Compared to the pristine monolayer B-As, the opening angle of the hyperboloid decreases with the applied tensile

https://doi.org/10.1021/acs.nanolett.3c04730
Nano Lett. 2024, 24, 2057−2062

strain (see Figure S11), leading to strongly trapped electric fields in the associated cone that are conducive to efficient energy transmission and improved directional propagation.

In summary, we have revealed in-plane hyperbolic polaritons in monolayer B-As that originate from two exciton resonances in combination with their anisotropic oscillator strengths along two in-plane principal axes. The enhanced interchain orbital hopping, resulting from the weaker asymmetric sp^3-like hybridization, gives rise to one extra exciton resonant peak at Λ in the Γ−Y **k**-path, in addition to the common peak at Γ as in B-P. The resonant peak at Γ exhibits a high tunability by strain. Especially, a biaxial tensile strain can move the Γ-point peak toward the Λ-point peak and merge into the same frequency, to significantly enhance the overall hyperbolicity and light adsorption. The merged exciton resonant peak can be further tuned across various frequency regimes by applying an additional anisotropic biaxial strain. Moreover, with electromagnetic numerical simulations, we obtain directly a variety of propagation patterns of hyperbolic polaritons based on dielectric functions obtained from ab initio calculations, which can be useful guidance for future experiments. In addition to B-As, other 2D group-V monolayer materials such as Sb and Bi also exhibit similar puckered lattice structures along with additional ferroelectric polarization.[44] Moreover, their band dispersions are likely to generate multiple excitonic resonances to induce hyperbolic polaritons, which we expect to also be tunable by strain.

■ ASSOCIATED CONTENT

Data Availability Statement

The data that support the findings of this study are available from the corresponding author upon request.

Supporting Information

The Supporting Information is available free of charge at https://pubs.acs.org/doi/10.1021/acs.nanolett.3c04730.

The difference in optical absorption spectra between B-As and B-P, the biaxial strain tunable exciton resonant peaks in B-As, tunable hyperbolicity in monolayer B-As with anisotropic biaxial strain, details of the Mott−Wannier model, and numerical simulations for exciton polaritons in monolayer B-As (PDF)

■ AUTHOR INFORMATION

Corresponding Authors

Hongwei Wang − *Institute of High Pressure Physics, School of Physical Science and Technology, Ningbo University, Ningbo 315211, China*; Email: wanghongwei@nbu.edu.cn

Tian Cui − *Institute of High Pressure Physics, School of Physical Science and Technology, Ningbo University, Ningbo 315211, China*; Email: cuitian@nbu.edu.cn

Tony Low − *Department of Electrical and Computer Engineering, University of Minnesota, Minneapolis, Minnesota 55455, United States*; orcid.org/0000-0002-5759-5899; Email: tlow@umn.edu

Feng Liu − *Department of Materials Science and Engineering, University of Utah, Salt Lake City, Utah 84112, United States*; orcid.org/0000-0002-3701-8058; Email: fliu@eng.utah.edu

Authors

Yuhan Zhong − *Interdisciplinary Center for Quantum Information, State Key Laboratory of Modern Optical Instrumentation, ZJU-Hangzhou Global Science and Technology Innovation Center, Zhejiang University, Hangzhou 310027, China*

Wei Jiang − *Centre for Quantum Physics, Key Laboratory of Advanced Optoelectronic Quantum Architecture and Measurement (MOE), School of Physics, Beijing Institute of Technology, Beijing 100081, China*

Simone Latini − *Nanomade, Department of Physics, Technical University of Denmark, 2800 Kongens Lyngby, Denmark*

Shengxuan Xia − *Key Laboratory for Micro/Nano Optoelectronic Devices of Ministry of Education and Hunan Provincial Key Laboratory of Low-Dimensional Structural Physics and Devices, School of Physics and Electronics, Hunan University, Changsha 410082, China*; orcid.org/0000-0002-3158-6257

Zhenglu Li − *Mork Family Department of Chemical Engineering and Materials Science, University of Southern California, Los Angeles, California 90089, United States*

Complete contact information is available at: https://pubs.acs.org/10.1021/acs.nanolett.3c04730

Author Contributions

H.W. and Y.Z. contributed equally to this work. H.W., F.L., and T.L. initialized and planned the project. H.W. performed the DFT calculations and data analysis. W.J. constructed the tight-binding model. Y.Z. conducted the electromagnetic numerical simulation. S.L. provided the theoretical support for the Mott−Wannier model. F.L. and T.L. supervised the whole project. H.W. and F.L. cowrote the paper. All authors contributed to the discussion of the results and preparation of the manuscript.

Funding

H.W. was supported by Program for Science and Technology Innovation Team in Zhejiang under Grant No. 2021R01004 and Zhejiang Provincial Natural Science Foundation of China (LD24F040001). F.L. is supported by US Department of Energy-Basic Energy Sciences (Grant No. DE-FG02-04ER46148). W.J. was supported by the NSF of China (Grant No. 12204037) and the Beijing Institute of Technology Research Fund Program for Young Scholars. T.L. acknowledges funding support from NSF/DMREF under Grant Agreement No. 1921629. Z.L. acknowledges the Seed Fund support from the Ershaghi Center for Energy Transition (E-CET) at the Viterbi School of Engineering, University of Southern California.

Notes

The authors declare no competing financial interest.

■ REFERENCES

(1) Fiori, G.; Bonaccorso, F.; Iannaccone, G.; Palacios, T.; Neumaier, D.; Seabaugh, A.; Banerjee, S. K.; Colombo, L. Electronics based on two-dimensional materials. *Nat. Nanotechnol.* **2014**, *9*, 768−779.

(2) Xia, F.; Wang, H.; Xiao, D.; Dubey, M.; Ramasubramaniam, A. Two-dimensional material nanophotonics. *Nat. Photonics* **2014**, *8*, 899−907.

(3) Lin, Z.; Huang, Y.; Duan, X. Van der Waals thin-film electronics. *Nat. Electron.* **2019**, *2*, 378−388.

(4) Lin, X.; Yang, W.; Wang, K. L.; Zhao, W. Two-dimensional spintronics for low-power electronics. *Nat. Electron.* **2019**, *2*, 274−283.

(5) Chernikov, A.; Berkelbach, T. C.; Hill, H. M.; Rigosi, A.; Li, Y.; Aslan, B.; Reichman, D. R.; Hybertsen, M. S.; Heinz, T. F. Exciton

binding energy and nonhydrogenic Rydberg series in monolayer WS_2. *Phys. Rev. Lett.* **2014**, *113*, 076802.
(6) Gibbs, H.; Khitrova, G.; Koch, S. Exciton-polariton light-semiconductor coupling effects. *Nat. Photonics* **2011**, *5*, 273−273.
(7) Mueller, T.; Malic, E. Exciton physics and device application of two-dimensional transition metal dichalcogenide semiconductors. *npj 2D Mater. Appl.* **2018**, *2*, 29.
(8) Sethi, G.; Zhou, Y.; Zhu, L.; Yang, L.; Liu, F. Flat-band-enabled triplet excitonic insulator in a diatomic kagome lattice. *Phys. Rev. Lett.* **2021**, *126*, 196403.
(9) Sethi, G.; Cuma, M.; Liu, F. Excitonic Condensate in Flat Valence and Conduction Bands of Opposite Chirality. *Phys. Rev. Lett.* **2023**, *130*, 186401.
(10) Li, Y.; Chernikov, A.; Zhang, X.; Rigosi, A.; Hill, H. M.; Van Der Zande, A. M.; Chenet, D. A.; Shih, E.-M.; Hone, J.; Heinz, T. F. Measurement of the optical dielectric function of monolayer transition-metal dichalcogenides: MoS_2, $MoSe_2$, WS_2, and WSe_2. *Phys. Rev. B* **2014**, *90*, 205422.
(11) Khatibi, Z.; Feierabend, M.; Selig, M.; Brem, S.; Linderälv, C.; Erhart, P.; Malic, E. Impact of strain on the excitonic linewidth in transition metal dichalcogenides. *2D Mater.* **2019**, *6*, 015015.
(12) Liu, X.; Guo, W. Shear strain tunable exciton dynamics in two-dimensional semiconductors. *Phys. Rev. B* **2019**, *99*, 035401.
(13) Rivera, P.; Yu, H.; Seyler, K. L.; Wilson, N. P.; Yao, W.; Xu, X. Interlayer valley excitons in heterobilayers of transition metal dichalcogenides. *Nat. Nanotechnol.* **2018**, *13*, 1004−1015.
(14) Lu, X.; Li, X.; Yang, L. Modulated interlayer exciton properties in a two-dimensional moiré crystal. *Phys. Rev. B* **2019**, *100*, 155416.
(15) Wilson, N. P.; Yao, W.; Shan, J.; Xu, X. Excitons and emergent quantum phenomena in stacked 2D semiconductors. *Nature* **2021**, *599*, 383−392.
(16) Basov, D.; Fogler, M.; García de Abajo, F. Polaritons in van der Waals materials. *Science* **2016**, *354*, aag1992.
(17) Low, T.; Chaves, A.; Caldwell, J. D.; Kumar, A.; Fang, N. X.; Avouris, P.; Heinz, T. F.; Guinea, F.; Martin-Moreno, L.; Koppens, F. Polaritons in layered two-dimensional materials. *Nat. Mater.* **2017**, *16*, 182−194.
(18) Wang, C.; Huang, S.; Xing, Q.; Xie, Y.; Song, C.; Wang, F.; Yan, H. Van der Waals thin films of WTe_2 for natural hyperbolic plasmonic surfaces. *Nat. Commun.* **2020**, *11*, 1158.
(19) Wang, H.; Low, T. Hyperbolicity in two-dimensional transition metal ditellurides induced by electronic bands nesting. *Phys. Rev. B* **2020**, *102*, 241104.
(20) Ma, W.; Alonso-González, P.; Li, S.; Nikitin, A. Y.; Yuan, J.; Martín-Sánchez, J.; Taboada-Gutiérrez, J.; Amenabar, I.; Li, P.; Vélez, S.; et al. In-plane anisotropic and ultra-low-loss polaritons in a natural van der Waals crystal. *Nature* **2018**, *562*, 557−562.
(21) Mrejen, M.; Yadgarov, L.; Levanon, A.; Suchowski, H. Transient exciton-polariton dynamics in WSe_2 by ultrafast near-field imaging. *Sci. Adv.* **2019**, *5*, eaat9618.
(22) Hu, F.; Luan, Y.; Scott, M.; Yan, J.; Mandrus, D.; Xu, X.; Fei, Z. Imaging exciton-polariton transport in $MoSe_2$ waveguides. *Nat. Photonics* **2017**, *11*, 356−360.
(23) Brar, V. W.; Jang, M. S.; Sherrott, M.; Kim, S.; Lopez, J. J.; Kim, L. B.; Choi, M.; Atwater, H. Hybrid surface-phonon-plasmon polariton modes in graphene/monolayer h-BN heterostructures. *Nano Lett.* **2014**, *14*, 3876−3880.
(24) Latini, S.; De Giovannini, U.; Sie, E. J.; Gedik, N.; Hübener, H.; Rubio, A. Phonoritons as hybridized exciton-photon-phonon excitations in a monolayer h-BN optical cavity. *Phys. Rev. Lett.* **2021**, *126*, 227401.
(25) Li, D.; Shan, H.; Rupprecht, C.; Knopf, H.; Watanabe, K.; Taniguchi, T.; Qin, Y.; Tongay, S.; Nuß, M.; Schröder, S.; et al. Hybridized exciton-photon-phonon states in a transition metal dichalcogenide van der Waals heterostructure microcavity. *Phys. Rev. Lett.* **2022**, *128*, 087401.
(26) Ma, W.; Shabbir, B.; Ou, Q.; Dong, Y.; Chen, H.; Li, P.; Zhang, X.; Lu, Y.; Bao, Q. Anisotropic polaritons in van der Waals materials. *InfoMat* **2020**, *2*, 777−790.
(27) Li, P.; Lewin, M.; Kretinin, A. V.; Caldwell, J. D.; Novoselov, K. S.; Taniguchi, T.; Watanabe, K.; Gaussmann, F.; Taubner, T. Hyperbolic phonon-polaritons in boron nitride for near-field optical imaging and focusing. *Nat. Commun.* **2015**, *6*, 7507.
(28) Dai, S.; Ma, Q.; Andersen, T.; Mcleod, A.; Fei, Z.; Liu, M.; Wagner, M.; Watanabe, K.; Taniguchi, T.; Thiemens, M.; et al. Subdiffractional focusing and guiding of polaritonic rays in a natural hyperbolic material. *Nat. Commun.* **2015**, *6*, 6963.
(29) Palermo, G.; Sreekanth, K. V.; Maccaferri, N.; Lio, G. E.; Nicoletta, G.; De Angelis, F.; Hinczewski, M.; Strangi, G. Hyperbolic dispersion metasurfaces for molecular biosensing. *Nanophotonics* **2020**, *10*, 295−314.
(30) Fang, W.; Yang, Y. Directional dipole radiations and long-range quantum entanglement mediated by hyperbolic metasurfaces. *Opt. Express* **2020**, *28*, 32955−32977.
(31) Sternbach, A.; Chae, S.; Latini, S.; Rikhter, A.; Shao, Y.; Li, B.; Rhodes, D.; Kim, B.; Schuck, P. J.; Xu, X.; et al. Programmable hyperbolic polaritons in van der Waals semiconductors. *Science* **2021**, *371*, 617−620.
(32) Wang, F.; Wang, C.; Chaves, A.; Song, C.; Zhang, G.; Huang, S.; Lei, Y.; Xing, Q.; Mu, L.; Xie, Y.; et al. Prediction of hyperbolic exciton-polaritons in monolayer black phosphorus. *Nat. Commun.* **2021**, *12*, 5628.
(33) Chen, Y.; Chen, C.; Kealhofer, R.; Liu, H.; Yuan, Z.; Jiang, L.; Suh, J.; Park, J.; Ko, C.; Choe, H. S.; et al. Black arsenic: a layered semiconductor with extreme in-plane anisotropy. *Adv. Mater.* **2018**, *30*, 1800754.
(34) Zhong, M.; Xia, Q.; Pan, L.; Liu, Y.; Chen, Y.; Deng, H.-X.; Li, J.; Wei, Z. Thickness-dependent carrier transport characteristics of a new 2D elemental semiconductor: black arsenic. *Adv. Funct. Mater.* **2018**, *28*, 1802581.
(35) Hybertsen, M. S.; Louie, S. G. Electron correlation in semiconductors and insulators: Band gaps and quasiparticle energies. *Phys. Rev. B* **1986**, *34*, 5390.
(36) Deslippe, J.; Samsonidze, G.; Strubbe, D. A.; Jain, M.; Cohen, M. L.; Louie, S. G. BerkeleyGW: A massively parallel computer package for the calculation of the quasiparticle and optical properties of materials and nanostructures. *Comput. Phys. Commun.* **2012**, *183*, 1269−1289.
(37) Rohlfing, M.; Louie, S. G. Electron-hole excitations and optical spectra from first principles. *Phys. Rev. B* **2000**, *62*, 4927.
(38) Marzari, N.; Mostofi, A. A.; Yates, J. R.; Souza, I.; Vanderbilt, D. Maximally localized Wannier functions: Theory and applications. *Rev. Mod. Phys.* **2012**, *84*, 1419.
(39) Liu, Z.; Wu, J.; Duan, W.; Lagally, M. G.; Liu, F. Electronic phase diagram of single-element silicon "strain" superlattices. *Phys. Rev. Lett.* **2010**, *105*, 016802.
(40) Chaves, A.; Azadani, J. G.; Alsalman, H.; Da Costa, D.; Frisenda, R.; Chaves, A.; Song, S. H.; Kim, Y. D.; He, D.; Zhou, J.; et al. Bandgap engineering of two-dimensional semiconductor materials. *NPJ. 2D Mater. Appl.* **2020**, *4*, 29.
(41) Si, C.; Sun, Z.; Liu, F. Strain engineering of graphene: a review. *Nanoscale* **2016**, *8*, 3207−3217.
(42) Zhang, Y.; Liu, F. Maximum asymmetry in strain induced mechanical instability of graphene: Compression versus tension. *Appl. Phys. Lett.* **2011**, *99*, 241908.
(43) Olsen, T.; Latini, S.; Rasmussen, F.; Thygesen, K. S. Simple screened hydrogen model of excitons in two-dimensional materials. *Phys. Rev. Lett.* **2016**, *116*, 056401.
(44) Zhong, S.; Zhang, X.; Liu, S.; Yang, S. A.; Lu, Y. Giant and nonanalytic negative piezoelectric response in elemental group-Va ferroelectric monolayers. *Phys. Rev. Lett.* **2023**, *131*, 236801.

https://doi.org/10.1021/acs.nanolett.3c04730
Nano Lett. 2024, 24, 2057−2062